

# Northumbria Research Link

Citation: Elkady, Mustafa, Elmarakbi, Ahmed, MacIntyre, John and Al Hariri, Mohammad (2017) Collision mitigation and vehicle transportation safety using integrated vehicle dynamics control systems. Journal of Traffic and Transportation Engineering (English Edition), 4 (1). pp. 41-60. ISSN 2095-7564

Published by: Elsevier

URL: <http://dx.doi.org/10.1016/j.jtte.2016.08.002>  
<<http://dx.doi.org/10.1016/j.jtte.2016.08.002>>

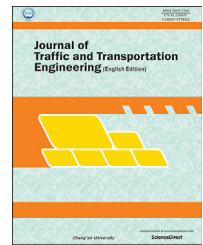
This version was downloaded from Northumbria Research Link:  
<http://nrl.northumbria.ac.uk/id/eprint/36094/>

Northumbria University has developed Northumbria Research Link (NRL) to enable users to access the University's research output. Copyright © and moral rights for items on NRL are retained by the individual author(s) and/or other copyright owners. Single copies of full items can be reproduced, displayed or performed, and given to third parties in any format or medium for personal research or study, educational, or not-for-profit purposes without prior permission or charge, provided the authors, title and full bibliographic details are given, as well as a hyperlink and/or URL to the original metadata page. The content must not be changed in any way. Full items must not be sold commercially in any format or medium without formal permission of the copyright holder. The full policy is available online: <http://nrl.northumbria.ac.uk/policies.html>

This document may differ from the final, published version of the research and has been made available online in accordance with publisher policies. To read and/or cite from the published version of the research, please visit the publisher's website (a subscription may be required.)

Available online at [www.sciencedirect.com](http://www.sciencedirect.com)

ScienceDirect

journal homepage: [www.elsevier.com/locate/jtte](http://www.elsevier.com/locate/jtte)

## Original Research Paper

# Collision mitigation and vehicle transportation safety using integrated vehicle dynamics control systems

Mustafa Elkady <sup>a,b</sup>, Ahmed Elmarakbi <sup>c,\*</sup>, John MacIntyre <sup>c</sup>,  
Mohammed Alhariri <sup>c</sup>

<sup>a</sup> School of Engineering, Lebanese International University, Beirut, Lebanon

<sup>b</sup> Faculty of Engineering, Ain Shams University, Cairo, Egypt

<sup>c</sup> Faculty of Engineering and Advanced Manufacturing, University of Sunderland, Sunderland, SR6 0DD, UK

## HIGHLIGHTS

- Integrated vehicle dynamics control systems for collisions improvement.
- Development of a new dynamics/crash mathematical model for vehicle collisions.
- Development of a new occupant-based lumped mass-spring-damper mathematical model.
- Vehicle response and occupant behaviour are captured and analysed accurately.

## ARTICLE INFO

## Article history:

Received 1 October 2015

Received in revised form

7 August 2016

Accepted 18 August 2016

Available online 5 January 2017

## Keywords:

Vehicle transportation safety

Collision mitigation

Vehicle dynamics and control

Mathematical modelling

Occupant kinematics

## ABSTRACT

The aim of this paper is to investigate the effect of vehicle dynamics control systems (VDCS) on both the collision of the vehicle body and the kinematic behaviour of the vehicle's occupant in case of offset frontal vehicle-to-vehicle collision. A unique 6-degree-of-freedom (6-DOF) vehicle dynamics/crash mathematical model and a simplified lumped mass occupant model are developed. The first model is used to define the vehicle body crash parameters and it integrates a vehicle dynamics model with a vehicle front-end structure model. The second model aims to predict the effect of VDCS on the kinematics of the occupant. It is shown from the numerical simulations that the vehicle dynamics/crash response and occupant behaviour can be captured and analysed quickly and accurately. Furthermore, it is shown that the VDCS can affect the crash characteristics positively and the occupant behaviour is improved.

© 2017 Periodical Offices of Chang'an University. Publishing services by Elsevier B.V. on behalf of Owner. This is an open access article under the CC BY-NC-ND license (<http://creativecommons.org/licenses/by-nc-nd/4.0/>).

\* Corresponding author. Tel.: +44 191 515 3877.

E-mail address: [ahmed.elmarakbi@sunderland.ac.uk](mailto:ahmed.elmarakbi@sunderland.ac.uk) (A. Elmarakbi).

Peer review under responsibility of Periodical Offices of Chang'an University.

<http://dx.doi.org/10.1016/j.jtte.2016.08.002>

2095-7564/© 2017 Periodical Offices of Chang'an University. Publishing services by Elsevier B.V. on behalf of Owner. This is an open access article under the CC BY-NC-ND license (<http://creativecommons.org/licenses/by-nc-nd/4.0/>).

## 1. Introduction

Vehicle dynamics control systems (VDCS) exist on the most modern vehicles and play important roles in vehicle ride, stability, and safety. For example, anti-lock brake system (ABS) is used to allow the vehicle to follow the desired steering angle while intense braking is applied (Bang et al., 2001; Yu et al., 2002). In addition, the ABS helps reducing the stopping distance of a vehicle compared to the conventional braking system (Celentano et al., 2003; Pasillas-Lépine, 2006). The active suspension control system (ASC) is used to improve the quality of the vehicle ride and reduce the vertical acceleration (Alleyne and Hedrick, 1995; Yue et al., 1988). From the view of vehicle transportation safety, nowadays, occupant safety becomes one of the most important research areas and the automotive industry increased their efforts to enhance the safety of vehicles. Seat belts, airbags, and advanced driver assistant systems (ADAS) are used to prevent a vehicle crash or mitigate vehicle collision when a crash occurs.

The most well-known pre-collision method is the advance driver assistant systems (ADAS). The aim of ADAS is to mitigate and avoid vehicle frontal collisions. The main idea of ADAS is to collect data from the road (i.e., traffic lights, other cars distances and velocities, obstacles, etc.) and transfer this information to the driver, warn the driver in danger situations and aid the driver actively in imminent collision (Gietelink et al., 2006; Seiler et al., 1998). There are different actions may be taken when these systems detect that the collision is unavoidable. For example, to help the driver actively, the braking force can be applied in imminent collision (Jansson et al., 2002), in addition, the brake assistant system (BAS) (Tamura et al., 2001) and the collision mitigation brake system (CMBS) (Sugimoto and Sauer, 2005) were used to activate the braking instantly based on the behaviour characteristics of the driver, and relative position of the most dangerous other object for the moment.

Vehicle crash structures are designed to be able to absorb the crash energy and control vehicle deformations, therefore simple mathematical models are used to represent the vehicle front structure (Emori, 1968). In this model, the vehicle mass is represented as a lumped mass and the vehicle structure is represented as a spring in a simple model to simulate a frontal and rear-end vehicle collision processes. Also, other analyses and simulations of vehicle-to-barrier impact using a simple mass spring model were established by Kamal (1970) and widely extended by Elmarakbi and Zu (2005, 2007) to include smart-front structures. To achieve enhanced occupant safety, the crash energy management system was explored by Khattab (2010). This study, using a simple lumped-parameter model, discussed the applicability of providing variable energy-absorbing properties as a function of the impact speed.

In terms of the enhancing crash energy absorption and minimizing deformation of the vehicle's structure, a frontal structure consisting of two special longitudinal members was designed (Witteman and Kriens, 1998; Witteman, 1999). This longitudinal member system was divided into two separate systems: the first, called the crushing part, guarantees the desired stable and efficient energy absorption; the other,

called the supporting part, guarantees the desired stiffness in the transverse direction. For high crash energy absorption and weight efficiency, new multi-cell profiles were developed (Kim, 2002). Various design aspects of the new multi-cell members were investigated and the optimization was carried out as an exemplary design guide.

The vehicle body pitches and drops at frontal impact are the main reason for the unbelted driver neck and head injury (Chang et al., 2006). Vehicle pitch and drop are normally experienced at frontal crash tests. They used a finite element (FE) method to investigate the frame deformation at full frontal impact and discussed the cause and countermeasures design for the issue of vehicle body pitch and drop. It found that the bending down of frame rails caused by the geometry offsets of the frame rails in vertical direction during a crash is the key feature of the pitching of the vehicle body.

The effect of vehicle braking on the crash and the possibility of using vehicle dynamics control systems to reduce the risk of incompatibility and improve the crash performance in frontal vehicle-to-barrier collision were investigated (Hogan and Manning, 2007). They proved that there was a slight improvement of the vehicle deformation once the brakes were applied during the crash. A multi-body vehicle dynamic model using ADAMS software, alongside with a simple crash model was generated in order to study the effects of the implemented control strategy.

Their study showed that the control systems were not able to significantly affect the vehicle dynamics in the offset barrier impact. In addition, it was found that in offset vehicle-to-vehicle rear-end collision, the ABS or direct yaw control (DYC) systems can stabilize the vehicle. However, these control systems affected each other and cannot work together at the same time.

The behaviour of a vehicle at high-speed crashes is enhanced by using active vehicle dynamics control systems (Elkady and Elmarakbi, 2012). A 6-degree-of-freedom (6-DOF) mathematical model was developed to carry out this study. In this model, vehicle dynamics was studied together with a vehicle crash structural dynamics and a validation of the vehicle crash structure of the proposed model was achieved. Four different cases of VDCS were applied to the model to predict the most effective one. An extension to this study, an occupant model has been developed and the effect of VDCS on the occupant kinematics has been analysed (Elkady and Elmarakbi, 2012).

The main aim of this research is to investigate the effect of the VDCS on vehicle collision mitigation, enhance vehicle crash characteristics, and improve occupant biodynamics responses in case of 50% vehicle-to-vehicle offset crash scenario. For that purpose, different seven cases of VDCS are applied to the vehicle model, there are three new cases which are not mentioned in the previous publications.

## 2. Methodology

A vehicle frontal collision can be divided into two main stages, the first one is a primary impact, and the second one is a secondary impact. The primary impact indicates the collision

between the front-end structure of the vehicle and an obstacle (another vehicle in this paper). The secondary impact is the interaction between the occupant and the restraint system and/or the vehicle interior due to vehicle collisions.

## 2.1. Vehicle dynamics/crash model

Using mathematical models in crash simulation is useful at the first design concept because rapid analysis is required at this stage. In addition, the well-known advantage of mathematical modelling provides a quick simulation analysis compared with FE models. In this paper, a 6-DOF vehicle dynamics/crash mathematical model, shown in Fig. 1(a), has been developed to optimize the VDCS, which will be embedded in the control unit, in impending impact at offset vehicle-to-vehicle crash scenarios for vehicle collision mitigation. The ABS and the ASC systems are co-simulated with a full car vehicle dynamic model and integrated with a front-end structure. It is worthwhile mentioning that vehicle components, which significantly affect the dynamics of a frontal impact, are modelled by lumped masses and nonlinear springs.

In this full-car model, the vehicle body is represented by lumped mass  $m$  and it has a translational motion in longitudinal direction ( $x$  axis), translational motion on vertical direction ( $z$  axis), pitching motion (around  $y$  axis), rolling motion (around  $x$  axis), and yawing motion in case of offset collision (around  $z$  axis at the point of impact). Four spring/damper units are used to represent the conventional vehicle suspension systems. Each unit has a spring stiffness  $k_s$  and a damping coefficient  $c$ . The subscripts  $f$ ,  $r$ ,  $R$  and  $L$  denote the front, rear, right and left wheels, respectively. The ASC system is co-simulated with the conventional suspension system to add or subtract an active force element  $u$ . The ABS is co-simulated with the mathematical model using a simple wheel model. The unsprung masses are not considered in this model and it is assumed that the vehicle moves in a flat-asphalted road, which means that the vertical movement of the tyres and road vertical forces can be neglected.

To represent the front-end structure of the vehicle, four non-linear springs with stiffness  $k_s$  are proposed: two springs represent the upper members (rails) and two springs represent lower members of the vehicle frontal structure. The subscript  $u$  denotes the upper rails while the subscript  $l$

denotes the lower rails. The bumper of the vehicle is represented by a lumped mass  $m_b$  and it has a longitudinal motion in the  $x$  direction and rotational motion for the non-impacted side of each bumper.

The general dimensions of the model are shown in Fig. 1(a), where  $l_f$ ,  $l_r$ ,  $l$  and  $h$  represent the longitudinal distance between the vehicle's CG and front wheels, the longitudinal distance between the CG and rear wheels, the wheel base and the high of the CG from the ground, respectively.  $a$  is the distance between the centre of the bumper and the right/left frontal springs;  $b$  is the distance between the CG and right/left wheels.

The free body diagram of the mathematical model is shown in Fig. 1(b), which represents the different internal and external forces applied on the vehicle body.  $F_s$ ,  $F_S$ ,  $F_b$ ,  $F_z$  and  $F_f$  are front-end non-linear spring forces, vehicle suspension forces, braking forces, normal forces and friction forces between the tyres and the road due to vehicle yawing, respectively.

**2.1.1. Equations of motion of vehicle-to-vehicle crash scenario**  
The model in the case of offset frontal vehicle-to-barrier is thirteen DOF namely longitudinal and vertical movements, pitching, rolling and yawing motions for each vehicle body, the longitudinal movement of the two bumpers as one part, and the rotational motion for the non-impacted side of each bumper. The two bumpers of each vehicle are considered as lumped masses, and dealt as one mass to transfer the load from one vehicle to another. Fig. 2 shows the vehicle model before and after collision in case of offset frontal vehicle-to-vehicle crash scenario. The equations of motion of the mathematical model shown in Fig. 2 are developed to study and predict the dynamic response of the primary impact of offset vehicle-to-vehicle crash scenario. Fig. 3 is used to describe the deformation of the front springs due to vehicle pitching around its CG and vehicle yawing around the point of impact for the two vehicles, respectively. Fig. 1 is also used to derive the equations of motion of the two vehicle models. The detailed equations of motion were created in a previous study by the authors (Elmarakbi et al., 2013).

## 2.1.2. Forces applied to the vehicle

There are different types of forces which are applied on the vehicle body. These forces are generated by crushing the front-

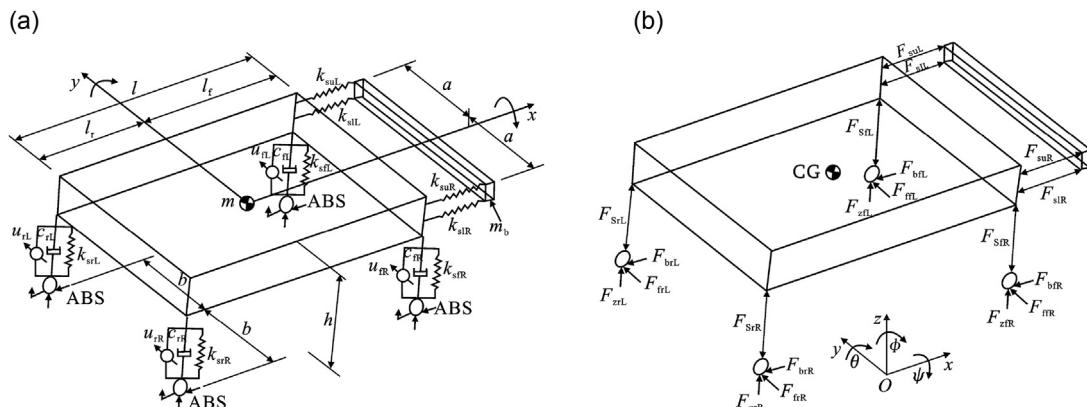


**Fig. 1 – Mathematical model. (a) 6-DOF vehicle dynamics/crash mathematical model. (b) Free body diagram of the mathematical model.**

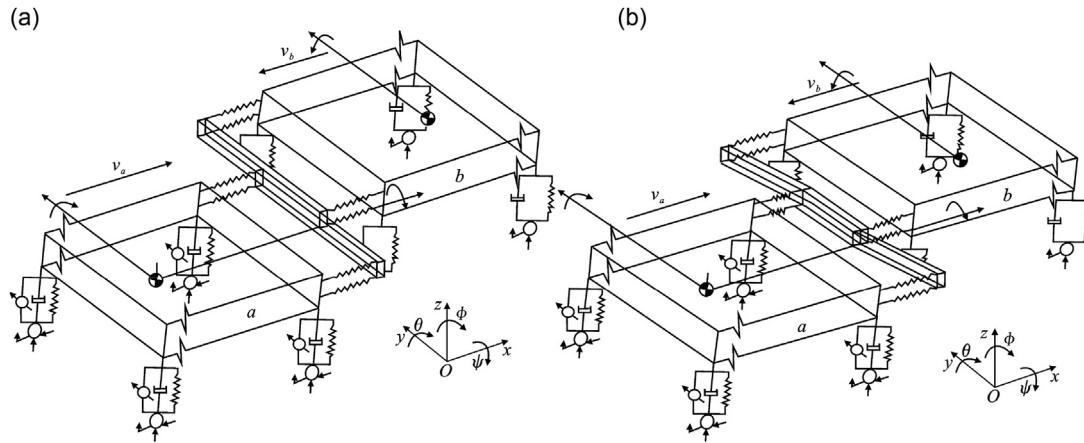


Fig. 2 – Vehicle models (offset frontal impact). (a) Before crash. (b) After crash.

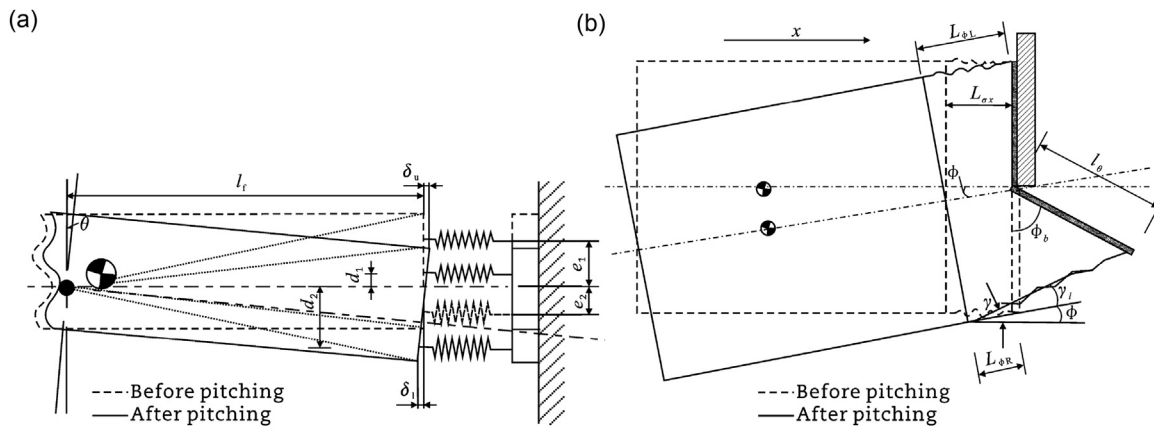


Fig. 3 – Front-end deformations before and after pitching. (a) For vehicle pitching. (b) For vehicle yawing.

end structure, conventional suspension system due to the movement of the vehicle body and the active control systems such as the ABS and ASC. The free body diagram shown in Fig. 1(b) illustrates these different forces and their directions.

To simulate the upper and lower members of the vehicle front-end structure, multi-stage piecewise linear force-deformation spring characteristics are considered. The non-linear springs used in the multi-body model ADAMS (Hogan and Manning, 2007) are taken to generate the  $n$  stage piecewise spring's characteristics as shown in Fig. 4(a), while the general relationship between the force and the deflection, Fig. 4(b), is used to calculate the force of the vehicle's front-end. The suspension forces of the vehicle body are also calculated.

The detailed equations of these forces and the validation of the vehicle dynamics–crash model was established in a previous study by the authors (Elkady and Elmarakbi, 2012). The validation is performed to ensure the validity of the model and is accomplished by comparing the mathematical model results with real test data and the results of the former ADAMS model. The validation showed that the mathematical model results are well matched with the other results.

## 2.2. Multi-body occupant model

In this section, occupant biodynamic is considered by modelling the occupant mathematically in order to be integrated with the vehicle mathematical model. The occupant model is proposed to be three-body model to capture its dynamic response, rotational events of the chest and head, due to different crash scenarios. The restraint system consists of seat belt, front and side airbags is presented by different spring-damper systems.

The occupant biodynamic model shown in Fig. 5 is developed in this study to evaluate the occupant kinematic behaviour in full and offset frontal crash scenarios. The human body model consists of three bodies with masses  $m_1$ ,  $m_2$  and  $m_3$ . The first body (lower body/pelvis) with mass  $m_1$ , represents the legs and the pelvic area of the occupant and it is considered to have a translation motion in the longitudinal direction and rotation motions (pitching, rolling and yawing) with the vehicle body. The second body (middle body/chest), with mass  $m_2$ , represents the occupant's abdominal area, the thorax area and the arms, and it is considered to have a translation motion in the longitudinal



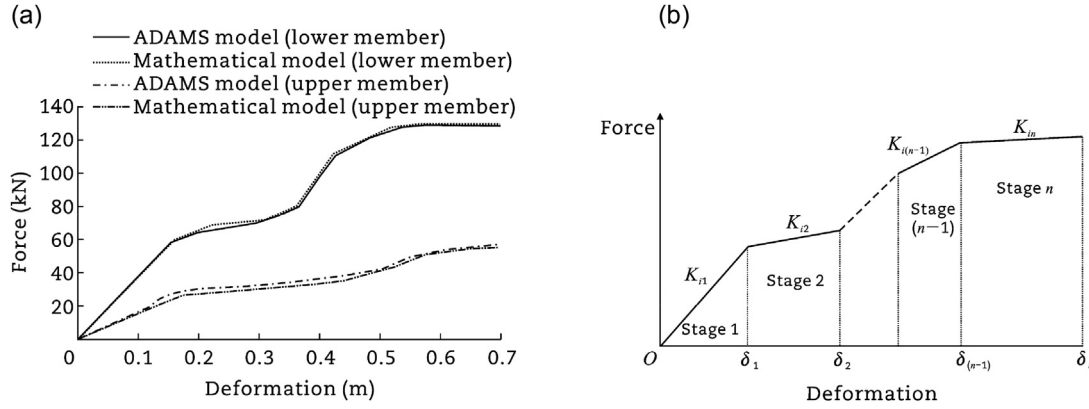


Fig. 4 – Force deformation characteristics. (a) For upper and lower rails. (b) General piecewise.

direction and a rotation motion around the pivot between the lower and middle bodies (pivot 1). The third body (upper body/head), with mass  $m_3$ , represents the head and neck of the occupant and it is considered to have a translation motion in the longitudinal direction and a rotational motion around the pivot between the middle and upper bodies (pivot 2).

A rotational coil spring is proposed at each pivot to represent the joint stiffness between the pelvic area and the abdominal area and between the thorax area and the neck/head area. The seatbelt is represented by two linear spring-damper units between the compartment and the occupant. The frontal and side airbags are each represented by two linear spring-damper units.

#### 2.2.1. Equation of motion (EOM) of the human body model

Fig. 6(a)–(c) shows the side, top and front views of the occupant model, respectively. POI in Fig. 6(b) means point of impact. For each figure, the positions of the occupant's three

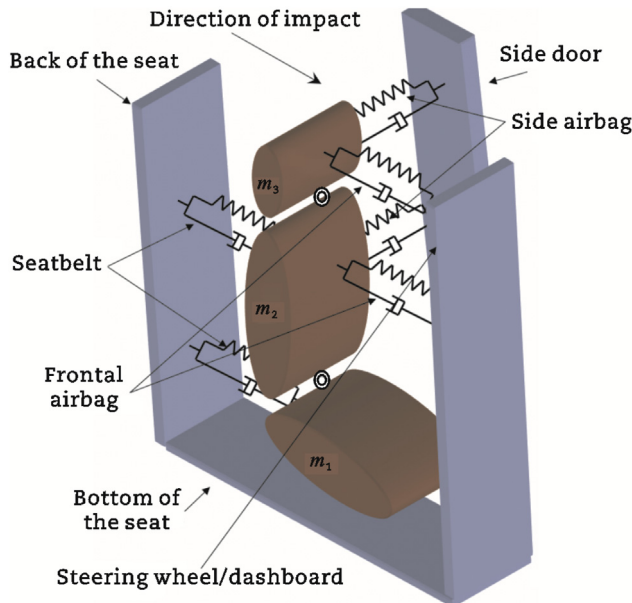


Fig. 5 – Multi-body occupant model.

bodies are illustrated before and after the crash. Lagrange's equations are used to describe the general motions of the multi-body human model.

The general motions of the multi-body human model are described using Lagrange's equations as follows

$$\frac{d}{dt} \left( \frac{\partial E}{\partial \dot{x}_1} \right) - \frac{\partial E}{\partial x_1} + \frac{\partial V}{\partial x_1} + \frac{\partial D}{\partial \dot{x}_1} = 0 \quad (1)$$

$$\frac{d}{dt} \left( \frac{\partial E}{\partial \dot{\theta}_2} \right) - \frac{\partial E}{\partial \theta_2} + \frac{\partial V}{\partial \theta_2} + \frac{\partial D}{\partial \dot{\theta}_2} = 0 \quad (2)$$

$$\frac{d}{dt} \left( \frac{\partial E}{\partial \dot{\theta}_3} \right) - \frac{\partial E}{\partial \theta_3} + \frac{\partial V}{\partial \theta_3} + \frac{\partial D}{\partial \dot{\theta}_3} = 0 \quad (3)$$

$$\frac{d}{dt} \left( \frac{\partial E}{\partial \dot{\psi}_2} \right) - \frac{\partial E}{\partial \psi_2} + \frac{\partial V}{\partial \psi_2} + \frac{\partial D}{\partial \dot{\psi}_2} = 0 \quad (4)$$

$$\frac{d}{dt} \left( \frac{\partial E}{\partial \dot{\psi}_3} \right) - \frac{\partial E}{\partial \psi_3} + \frac{\partial V}{\partial \psi_3} + \frac{\partial D}{\partial \dot{\psi}_3} = 0 \quad (5)$$

where  $E$ ,  $V$  and  $D$  are the kinetic energy, potential energy and the Rayleigh dissipation function of the system, respectively,  $x_1$ ,  $\theta_2$ ,  $\theta_3$ ,  $\psi_2$  and  $\psi_3$  are the longitudinal movement of the occupant's lower body, the rotational angle of the occupant's middle body about  $y$  axis, the rotational angle of the occupant's upper body about  $y$  axis, the rotational angle of the occupant's middle body about  $x$  axis and the rotational angle of the occupant's upper body about  $x$  axis, respectively, hence,  $\dot{x}_1$ ,  $\dot{\theta}_2$ ,  $\dot{\theta}_3$ ,  $\dot{\psi}_2$  and  $\dot{\psi}_3$  are their associated velocities, respectively.

The kinetic energy of the system can be written as

$$E = \frac{m_1 v_1^2}{2} + \frac{m_2 v_2^2}{2} + \frac{m_3 v_3^2}{2} + \frac{I_1 (\dot{\theta}^2 + \dot{\phi}^2 + \dot{\psi}^2)}{2} + \frac{I_2 (\dot{\theta}_2^2 + \dot{\psi}_2^2)}{2} + \frac{I_3 (\dot{\theta}_3^2 + \dot{\psi}_3^2)}{2} \quad (6)$$

where  $v_1$ ,  $v_2$  and  $v_3$  are the equivalent velocities of the lower, middle and upper bodies of the occupant, respectively,  $I_1$ ,  $I_2$  and  $I_3$  are the rotational moment of inertia of the lower, middle and upper bodies about the CG of each body, respectively. It is assumed that the rotational moment of inertia of each body around  $x$ ,  $y$  and  $z$  axes are the same.  $\dot{\theta}$ ,  $\dot{\phi}$  and  $\dot{\psi}$  represent the vehicle body pitching, yawing and rolling

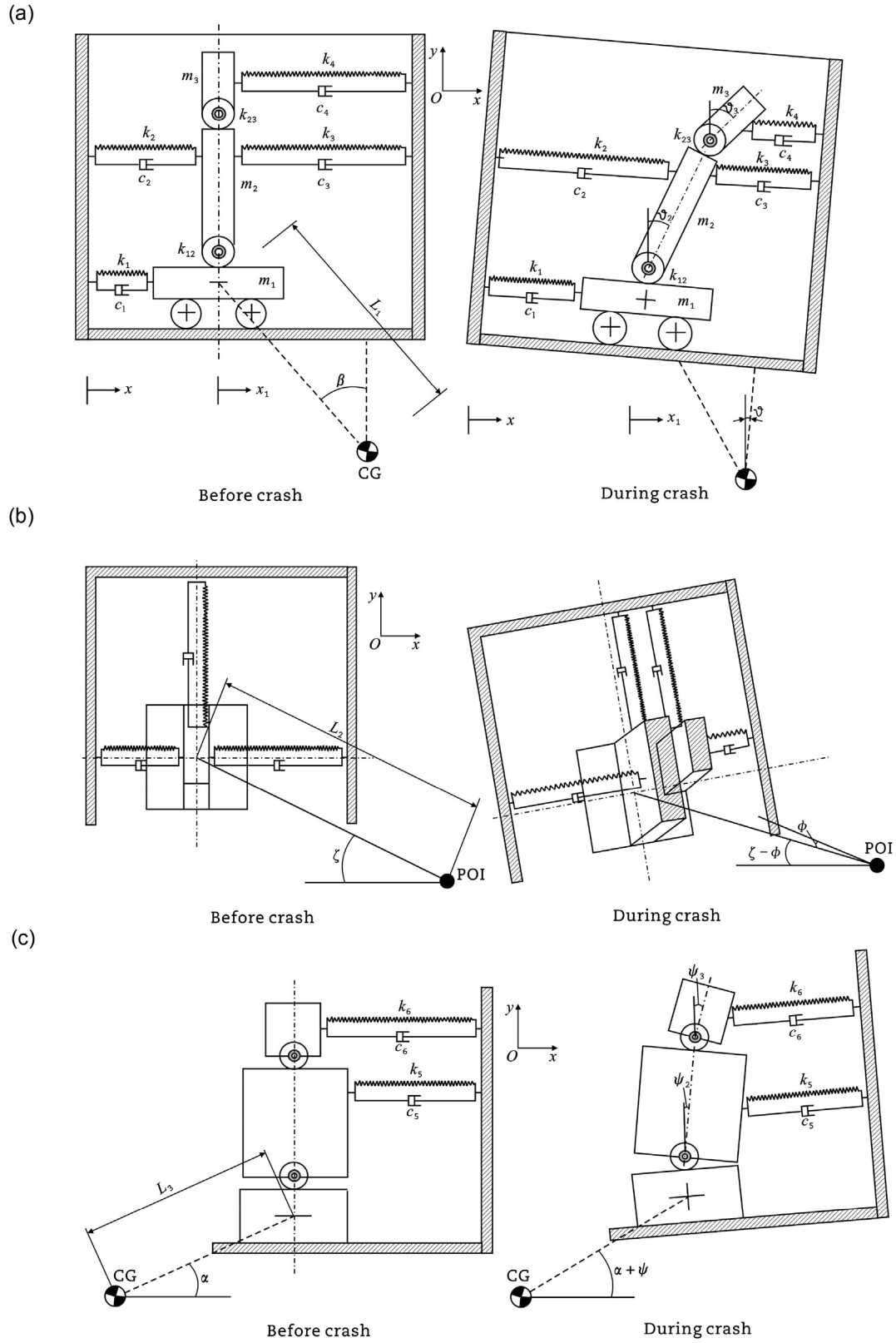


Fig. 6 – Occupant model. (a) Side view. (b) Top view. (c) Frontal view.

velocities, respectively. The equivalent velocities of the three bodies of the occupant can be calculated as follows

$$v_1^2 = \dot{X}_{m_1}^2 + \dot{Y}_{m_1}^2 + \dot{Z}_{m_1}^2 \quad (7)$$

where the displacement of the lower body in x direction can be calculated using Fig. 7 as

$$X_{m_1} = x_1 + L_1[\sin(\beta) - \sin(\beta - \theta)] - L_2[\cos(\zeta - \phi) - \cos(\zeta)] \quad (8)$$

The velocity of the lower body in x direction can be written as

$$\dot{X}_{m_1} = \dot{x}_1 + L_1 \dot{\theta} \cos(\beta - \theta) - L_2 \dot{\phi} \sin(\zeta - \phi) \quad (9)$$

The displacement and velocity of the lower body in y direction can be calculated as

$$Y_{m_1} = L_2 [\sin(\zeta) - \sin(\zeta - \phi)] + L_3 [\cos(\alpha) - \cos(\alpha + \psi)] \quad (10)$$

$$\dot{Y}_{m_1} = L_2 \dot{\phi} \cos(\zeta - \phi) + L_3 \dot{\psi} \sin(\alpha + \psi) \quad (11)$$

The displacement and velocity of the lower body in z direction can be calculated as

$$Z_{m_1} = z + L_1 [\cos(\beta - \theta) - \cos(\beta)] + L_3 [\sin(\alpha + \psi) - \sin(\alpha)] \quad (12)$$

$$\dot{Z}_{m_1} = L_1 \dot{\theta} \sin(\beta - \theta) + L_3 \dot{\psi} \cos(\alpha + \psi) \quad (13)$$

Substituting Eqs. (9), (11) and (13) in Eq. (7), the equivalent velocity of the lower body can be determined. By repeating the previous steps of these equations (Eqs. (8)–(13)), the equivalent velocities of the middle and upper bodies can be calculated.

Where  $X_m$  is the resultant longitudinal displacement in x direction,  $Y_m$  is the resultant vertical displacement in y direction and  $Z_m$  is the resultant vertical displacement. The subscript 1 is for lower body, 2 is for middle body and 3 is for upper body.  $L_1$  is the distance from the vehicle's y axis to the lower body's CG,  $L_2$  is the distance between the point of impact and the CG of the lower body, and  $L_3$  is the distance from the vehicle's x axis to the lower body's CG. It is assumed that  $L_1$ ,  $L_2$  and  $L_3$  are constant due to the insignificant change of their

lengths during the crash.  $\beta$  is the angle between the vertical centreline of the vehicle z axis and the line between the vehicle's y axis and the CG of the lower body ( $L_1$ ).  $\zeta$  is the angle between the longitudinal centreline of the vehicle x axis and the line between the point of impact and the CG of the lower body ( $L_2$ ).  $\alpha$  is the angle between the vertical centreline of the vehicle z axis and the line between the vehicle's x axis and the CG of the lower body ( $L_3$ ).

By substituting the equivalent velocities of the three bodies in Eq. (6), the kinetic energy can be obtained. Using Fig. 6 the potential energy of the system can be written as

$$\begin{aligned} V = & m_1 g [h + z + L_1 (\cos(\beta - \theta) - \cos(\beta))] \\ & + m_2 g \left[ h + z + L_1 (\cos(\beta - \theta) - \cos(\beta)) + \frac{l_2}{2} \cos(\theta_2) \right. \\ & \left. - \frac{l_2}{2} (1 - \cos(\psi_2)) \right] + m_3 g \left[ h + z + L_1 (\cos(\beta - \theta) - \cos(\beta)) \right. \\ & \left. + l_2 \cos(\theta_2) - l_2 (1 - \cos(\psi_2)) + \frac{l_3}{2} \cos(\theta_3) - \frac{l_3}{2} (1 - \cos(\psi_3)) \right] \\ & + \frac{1}{2} (F_{k1} \delta_1 + F_{k2} \delta_2 + F_{k3} \delta_3 + F_{k4} \delta_4 + F_{k5} \delta_5 + F_{k6} \delta_6 + F_{k12\theta} \delta_{12\theta} \\ & + F_{k12\psi} \delta_{12\psi} + F_{k23\theta} \delta_{23\theta} + F_{k23\psi} \delta_{23\psi}) \end{aligned} \quad (14)$$

where  $h$  is the vehicle's CG height and  $z$  is the vertical displacement of the vehicle body,  $F_{k1}$ ,  $F_{k2}$ ,  $F_{k3}$ ,  $F_{k4}$ ,  $F_{k5}$  and  $F_{k6}$  are the forces generated from the lower seatbelt spring, the upper seatbelt spring, the lower frontal airbag spring, the upper frontal airbag spring, the lower side airbag spring, the upper side airbag spring, respectively.  $F_{k12\theta}$  and  $F_{k12\psi}$  are the forces generated from the rotational spring between the middle and lower body around y and x axes, respectively.  $F_{k23\theta}$

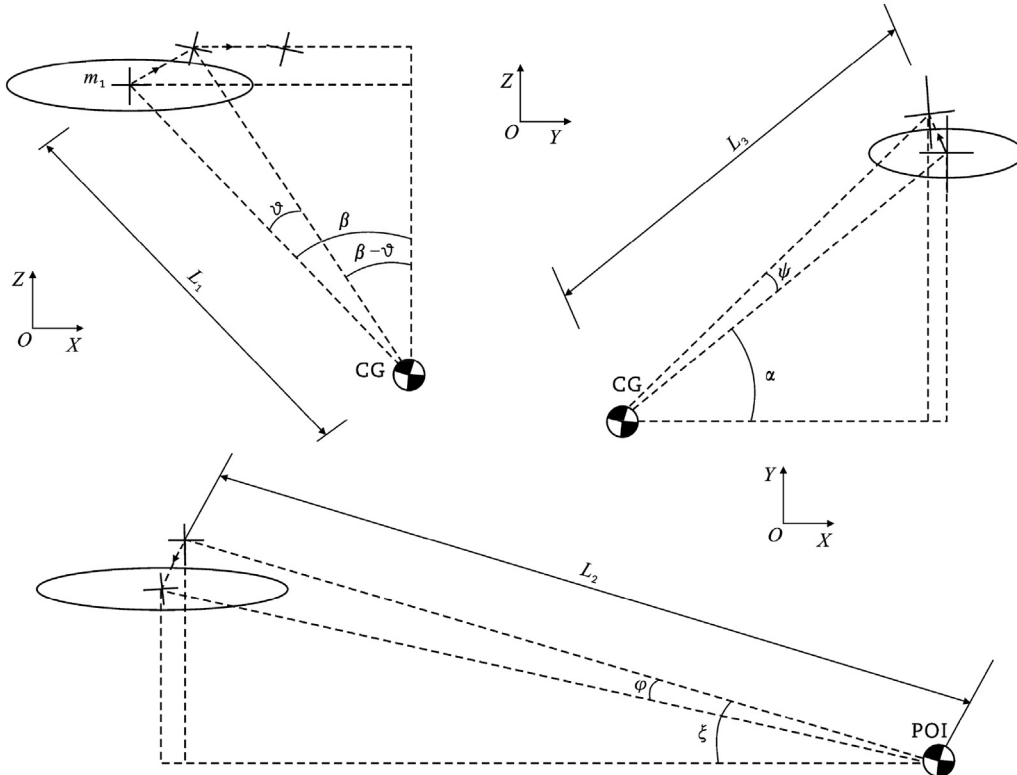


Fig. 7 – A schematic diagram of the occupant's lower body movement during impact.



and  $F_{k23\psi}$  are the forces generated from the rotational spring between the upper and middle body around  $y$  and  $x$  axes, respectively.  $\delta_1, \delta_2, \delta_3, \delta_4, \delta_5$  and  $\delta_6$  represent the total deflection of the lower seatbelt spring, of the upper seatbelt spring, of the lower frontal airbag spring, of the upper frontal airbag spring, of the lower side airbag spring, of the upper side airbag spring, respectively.  $\delta_{12\theta}$  and  $\delta_{12\psi}$ ,  $\delta_{23\theta}$  and  $\delta_{23\psi}$  are the deflection of the rotational spring between the lower and middle body around  $y$  and  $x$  axes and the deflection of the rotational spring between the middle and upper body around  $y$  and  $x$  axes, respectively.

The Rayleigh dissipation function can be written as follow

$$D = \frac{1}{2} (F_{c1}\dot{\delta}_1 + F_{c2}\dot{\delta}_2 + F_{c3}\dot{\delta}_3 + F_{c4}\dot{\delta}_4 + F_{c5}\dot{\delta}_5 + F_{c6}\dot{\delta}_6) \quad (15)$$

where  $F_{c1}, F_{c2}, F_{c3}, F_{c4}, F_{c5}$  and  $F_{c6}$  are the forces generated from the lower seatbelt, the upper seatbelt, the lower frontal airbag, the upper frontal airbag, the lower side airbag, and the upper side airbag dampers, respectively.  $\dot{\delta}_1, \dot{\delta}_2, \dot{\delta}_3, \dot{\delta}_4, \dot{\delta}_5$ , and  $\dot{\delta}_6$  are the associated velocities of the  $\delta_1, \delta_2, \delta_3, \delta_4, \delta_5$  and  $\delta_6$ , respectively.

The forces  $F_{ki}$  and  $F_{ci}$  ( $i = 1, 2, \dots$ ) are calculated as

$$F_{ki} = k_i \delta_i \quad (16)$$

$$F_{ci} = c_i \dot{\delta}_i \quad (17)$$

In order to get the components of Eqs. (1)–(5) the differentiation of the kinetic energy, potential energy and Rayleigh dissipation function are determined. To solve these equations, they need to be re-arranged in an integratable form and then rewritten in a matrix form as follow

$$\mathbf{A}\ddot{\mathbf{B}} = \mathbf{C} \quad (18)$$

$$\ddot{\mathbf{B}} = [\ddot{x}_1 \ddot{\theta}_2 \ddot{\theta}_3 \ddot{\psi}_2 \ddot{\psi}_3]^T$$

The final form then can be written as

$$\ddot{\mathbf{B}} = \mathbf{A}^{-1}\mathbf{C} \quad (19)$$

Different occupant bodies' responses ( $x_1, \theta_2, \theta_3, \psi_2$  and  $\psi_3$ ) can be determined by solving Eq. (19) numerically.

### 2.2.2. Occupant model validation

The occupant model has been validated by comparing its results with the former finite element human model and crash

test. To ensure that the input crash data applied to the dummy and the occupant in the finite element model match the input data in the mathematical model, the vehicle decelerations in all cases (mathematical model, finite element model and real test) are compared as depicted in Fig. 8. The same initial crash conditions are adapted in the mathematical model to be the same as in the FE model and the real test. It is observed that the deceleration of the mathematical model shows outstanding agreement with the real test and the finite element model results with respect to peak values and the timing of the curves.

Similarly, Fig. 9 shows the chest deceleration-time histories of the real test, finite element and mathematical models. The values and trends of the three different chest deceleration curves are well-matched. The maximum deceleration of the occupant chest in the mathematical model is a slightly lower compared to the real test data, while it is a slightly higher compared to the finite element model. In addition, there is a small shifting in this peak value compared with the other results. This is due to the modelling simplification of the airbag used in the mathematical models.

In the same way, the head deceleration results of the occupant models are presented in Fig. 10. Although the general trends and slopes of the three different results are well matched, there is a small difference in the peak value of the mathematical model compared with both finite element and real test results. A small shifting of the head deceleration peak value is also observed here for both finite element and mathematical models by different values compared with the real test data.

## 3. Numerical simulations

Seven different cases of VDCS are investigated in this section and their associated results are compared with the free rolling case scenario. These different VDCS cases are described as follows.

Case 1: free rolling – in this case the vehicle collides with a barrier/vehicle without applying any types of control.

Case 2: ABS – in this case the anti-lock braking system is applied before and during the collision.

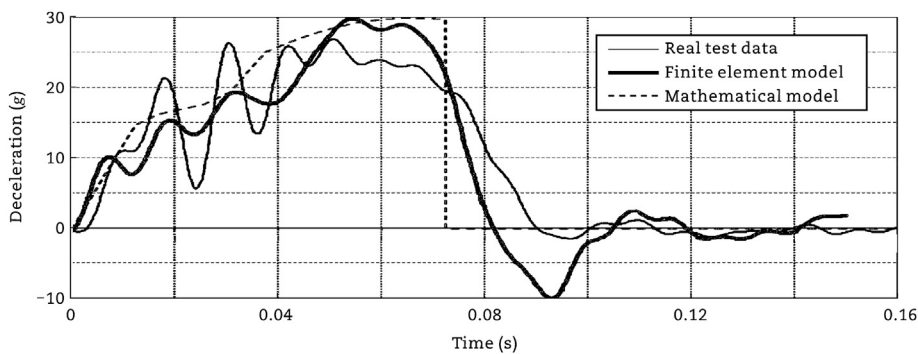


**Fig. 8 – Comparisons of the vehicle body deceleration results among a previous finite model, real test and the mathematical model.**

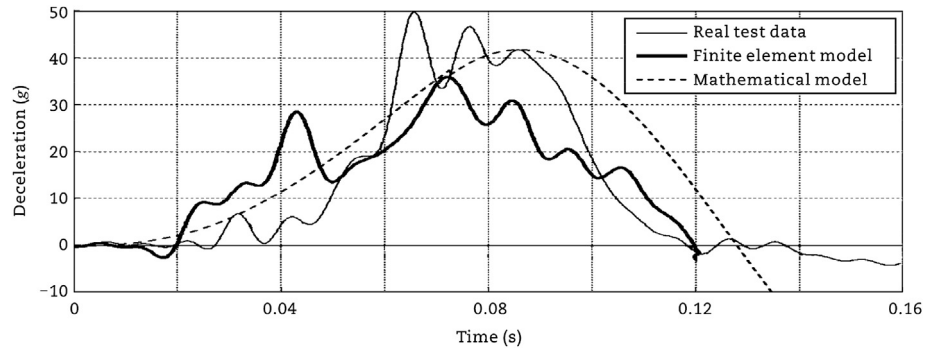


**Fig. 9 – Comparisons of the chest deceleration results among a previous finite element model, a real test and 3-body mathematical model.**

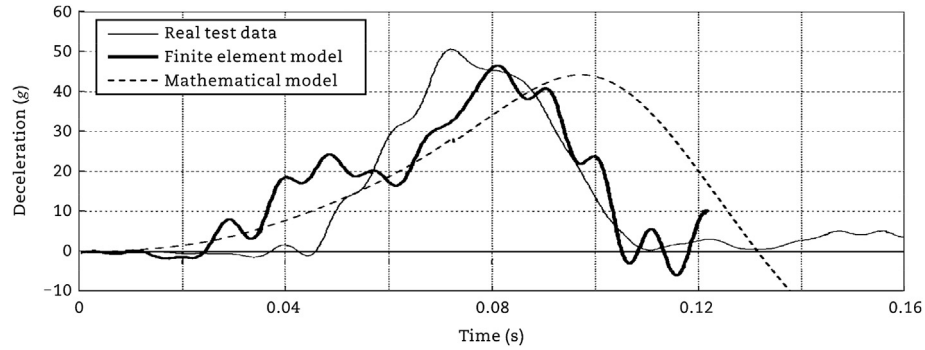


**Fig. 10 – Comparisons of the head deceleration results among a previous finite element model, a real test and a 3-body mathematical model.**

Case 3: ABS + ASC – the ASC system is integrated with the ABS to increase the vertical normal force on the road (Ori et al., 2011) and hence increase the braking force.

Case 4: ABS + frontal active suspension control (FASC) – the ASC system is integrated with the ABS on the front wheels only.

Case 5: ABS + anti-pitch control (APC) – the APC system is integrated with the ABS using the ACS to keep the vehicle in a horizontal position before the crash by applying an active force element on the front and rear wheels in upward and downward directions, respectively.

Case 6: ABS + UPC – in this case, the vehicle is taken a reverse pitching angle before crash using an ASC system.

Case 7: ABS DYC – the braking force is used to be applied to individual wheels to reduce the yawing moment of the vehicle body.

### 3.1. Primary impact results

The primary impact simulation results for offset vehicle-to-vehicle crash scenario are demonstrated in this section. The

**Table 1 – Values of the different parameters used in primary impact simulations.**

Parameter	$m$ (kg)	$I_{yy}$ (kg·m <sup>2</sup> )	$I_{xx}$ (kg·m <sup>2</sup> )	$I_{zz}$ (kg·m <sup>2</sup> )	$I_{bzz}$ (kg·m <sup>2</sup> )	$k_{SfR} = k_{SfL}$ (kN/m)	
Value	1200	1490	350	1750	40	18.25	
Parameter	$k_{SrR} = k_{SrL}$ (kN/m)	$c_{fR} = c_{fL}$ (N·s/m)	$c_{rR} = c_{rL}$ (N·s/m)	$l_f$ (m)	$l_r$ (m)	$h$ (m)	$l_a$ (m)
Value	13.75	1100	900	1.185	1.580	0.452	1.20
Parameter	$l_b$ (m)						$b_i = b_o$ (m)
Value	0.85						0.8

values of different parameters used in numerical simulations are given in Table 1 (Alleyne, 1997), where  $I_{yy}$ ,  $I_{xx}$ ,  $I_{zz}$  and  $I_{bzz}$  are the moments of inertia of the vehicle body about y, x and z axes and the moment of inertia of the rotation part of the bumper (the part of the bumper rotated with the non-impacted side of the vehicle due to offset collisions) about z axis at the point of impact, respectively. The effect of the different cases of VDCS on vehicle collision mitigation is also investigated. In addition, the effect of the control systems on the other vehicle (vehicle (b)) is discussed. Fig. 11 shows the impacted side of the front-end structure's deformation-time histories for vehicle (a) for all different VDCS cases. It is noticed that the deformation increased to reach its maximum value (different for each case) and then decreased slightly due to front-end springs rebound. The minimum deformation is obtained in the Case 3 when the ASC is applied along with ABS. The maximum reduction of 50 mm is observed in this case and a reduction of 30 mm is shown in Case 6, while a reduction of about 25 mm is obtained in Cases 2, 4 and 5 compared with the free rolling case. On the other hand, Case 7 (ABS + DYC) produced a higher deformation with a total reduction of about 15 mm. Although 50 mm is relatively small compared with the total deformation, this reduction may help prevent the compartment to be reached. The integrated control of the

ASC with the ABS aims to increase the braking force by increasing the vertical load to obtain a minimum stopping distance. It is worth mentioning that the application of the ASC control system (Case 3) helps reducing the maximum deformation of the front-end structure as shown in Fig. 11. For vehicle (b), the maximum deformation is almost the same with very small and insignificant values for all cases of VDCS, and this means the control systems have no great effect on the front-end deformation of the other vehicle during the offset collision.

The deceleration-time histories of the vehicle body for all cases of vehicle (a) are presented in Fig. 12. The deceleration-time history can be divided into three stages. The first stage represents the increase of the vehicle's deceleration before the front left wheel reaches the barrier. In this stage the highest deceleration value is observed in Case 3. In the other cases, a slight higher deceleration is also noticed compared with the free rolling case. In the second stage, the front left wheel reaches the barrier and stop moving, therefore its braking effects is vanished. At the beginning of this stage a rapid reduction in the vehicle body deceleration occurs (arrow 1, Fig. 12). This deceleration drop does not appear in the free rolling case while there is no applied braking. During the second stage, it is noticed that the minimum deceleration is still in Case 1, while the maximum

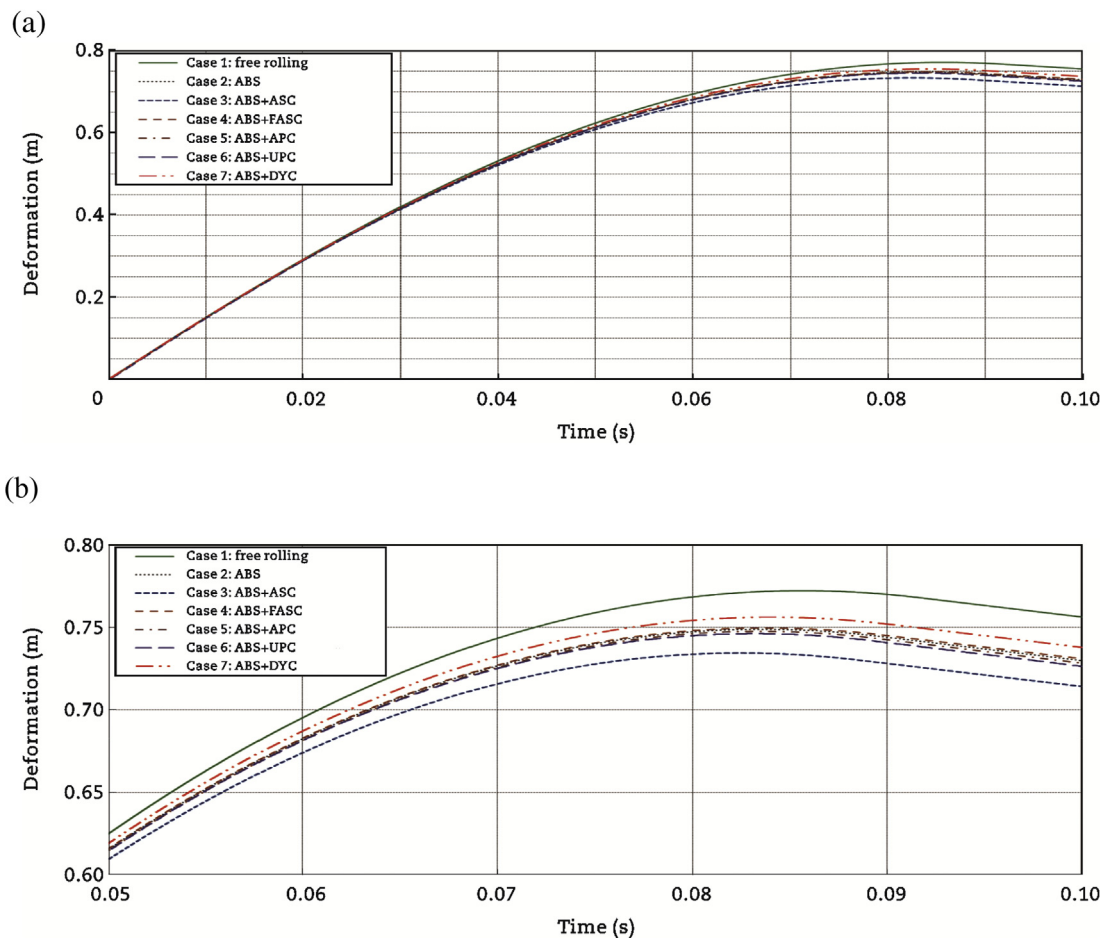


Fig. 11 – Deformation of the front-end structure (offset frontal vehicle-to-vehicle impact). (a) Vehicle (a). (b) (Enlarge scale) vehicle (a).

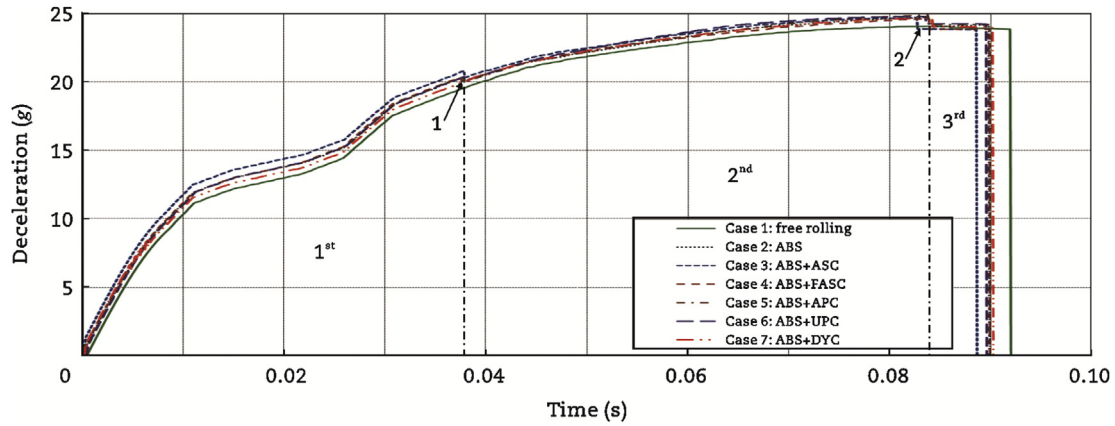


Fig. 12 – Vehicle body deceleration (offset frontal vehicle-to-vehicle impact), vehicle (a).

deceleration is almost the same for all other cases. At the end of this stage, the vehicle stops and starts moving in the opposite direction. In addition, the braking force changes its direction and another drop in the vehicle deceleration is noticed as shown in Fig. 12 (arrow 2). At the third stage, a condition of allowing the front-end springs to be rebounded for a very short time is applied during the simulation analysis. During this stage, the vehicle moves back and the deformation of the front-end decreases as shown in Fig. 12. At the end of this stage, the non-linear front-end springs are deactivated and the vehicle's deceleration suddenly dropped to a value of zero. This fast drop is due to the assumption of immediate stopping the effect front-end springs after a very short time of rebound.

An insignificant increase of the vehicle deceleration in all VDCS cases is observed in the other vehicle (b) compared with the free rolling case. The maximum values of the vehicle deceleration in a vehicle (b) are also almost the same for all the VDCS cases.

Fig. 13 shows the vehicle's pitch angle-time histories for all cases of vehicle (a). The VDCS is applied 1.5 s before the collision, therefore, the vehicle body impacts the barrier at different values of pitch angles according to each case as

shown in Fig. 13. The vehicle's pitch angle then reaches its maximum values (normally after the end of the crash) according to each case. Following this, the pitch angle reduces to reach negative values and then bounces to reach its steady-state condition. In the offset crash scenario, vehicle body pitching angle is generated due to the difference in impact forces between the upper and lower front-end members of the impacted side in the free rolling case. The additional pitching moment is generated from the braking force in the other VDCS cases. The maximum pitch angle is observed in Case 2 followed by Cases 7, 4, 1, 5, 3 and finally Case 6. In Case 6, a notable reduction of about 6.5 deg compared with Case 1 and about 12 deg, compared with Case 2 are observed.

A rolling moment of the vehicle body is generated during the crash due to the different values of the component of the left frontal springs' forces in y direction and from the friction between the ground and the tyres due to the yaw motion. At the end of the collision, the pitching and rolling moments are ended and the vehicle is controlled by the tyres and suspension forces. The vehicle's rear wheels left the ground during the vehicle pitching and the left wheels (front and rear) left the ground as well during the vehicle rolling. At this moment, three

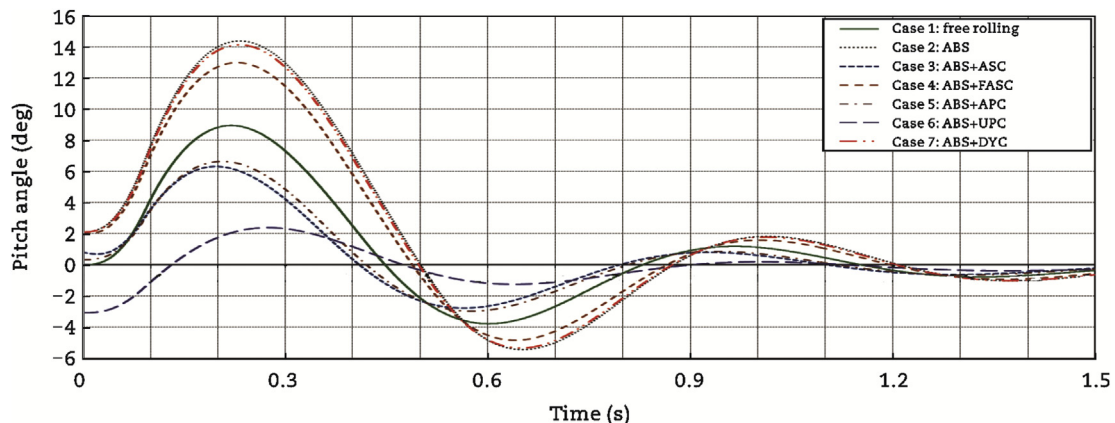


Fig. 13 – Vehicle body pitch angle (offset frontal vehicle-to-vehicle impact), vehicle (a).

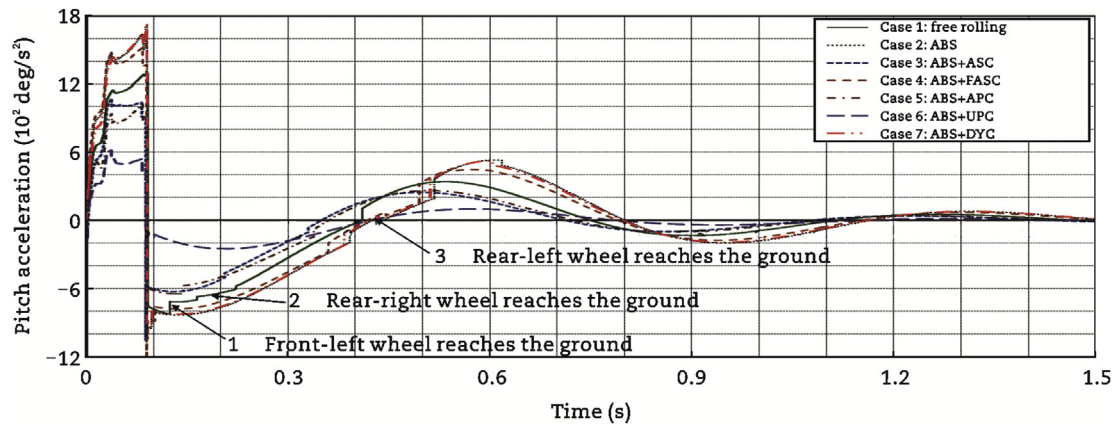


Fig. 14 – Vehicle body pitch acceleration (offset frontal vehicle-to-vehicle impact), vehicle (a).

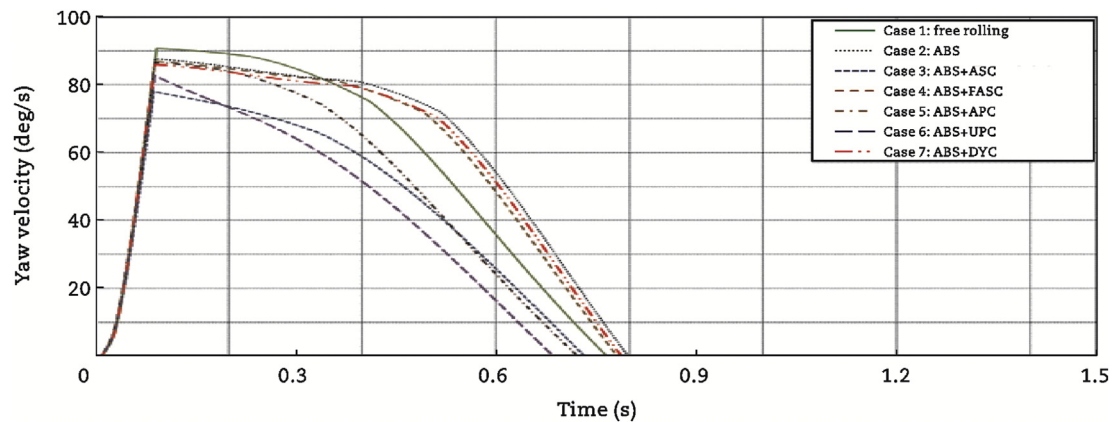


Fig. 15 – Vehicle body yaw velocity (offset frontal vehicle-to-vehicle impact), vehicle (a).

wheels of the vehicle are not contacted with the ground with different distances. This explains the different sudden changes of the vehicle pitching acceleration when each wheel re-contact the ground (look at the arrows referred to Case 1 in Fig. 14).

The vehicle body pitching acceleration is also depicted in Fig. 14 for all seven cases for vehicle (a). The vehicle maximum pitching acceleration is observed in Cases 2, 4 and 7, whilst the lowest value is detected in case 6 (ABS + UPC). Compared with Case 1 (free rolling) and case 2 (ABS), a reduction of about 670  $\text{deg/s}^2$  and about 950  $\text{deg/s}^2$ , respectively, are obtained in Case 6 (ABS + UPC).

Similarly, the pitch angle and pitch acceleration-time histories for vehicle (b) are obtained. It is noticed that there is no difference between the results of the seven crash scenarios. That means the different applied cases of the VDCS on vehicle (a) do not affect the pitching event of vehicle (b) in case of offset collision.

Fig. 15 shows the vehicle yaw velocity-time histories for all seven cases of vehicle (a). The vehicle yaw velocity is equal to zero before the crash, then it changes in three different stages:

firstly, it increases rapidly to reach its maximum value; secondly, it decreases slowly for a different period of time related to each case; and thirdly it decreases gradually to reach zero. In the first stage, the rapid increase in the yaw velocity is due to the high yawing acceleration (Fig. 16) caused by the one side impacted spring. At the end of the collision, the rear wheels left the ground due to the vehicle pitching and the front-left wheel left the ground due to the vehicle rolling and hence the vehicle is controlled by the front-right wheel only. In the second stage, the decrease in the vehicle's yaw velocity occurred due to the friction force between the front-rear tyre and the ground. The period of this stage is different for each case and it mainly depends on the maximum pitching angle. During the second stage, the front-left wheel re-contacts the ground. Stage 3 begins when the rear wheels start contacting the ground generating yaw moments in the opposite direction. This is causing a reduction of the vehicle yawing velocity with a higher rate than the decreasing of velocity rate in the second stage. Because of the maximum vehicle front-end deformation is



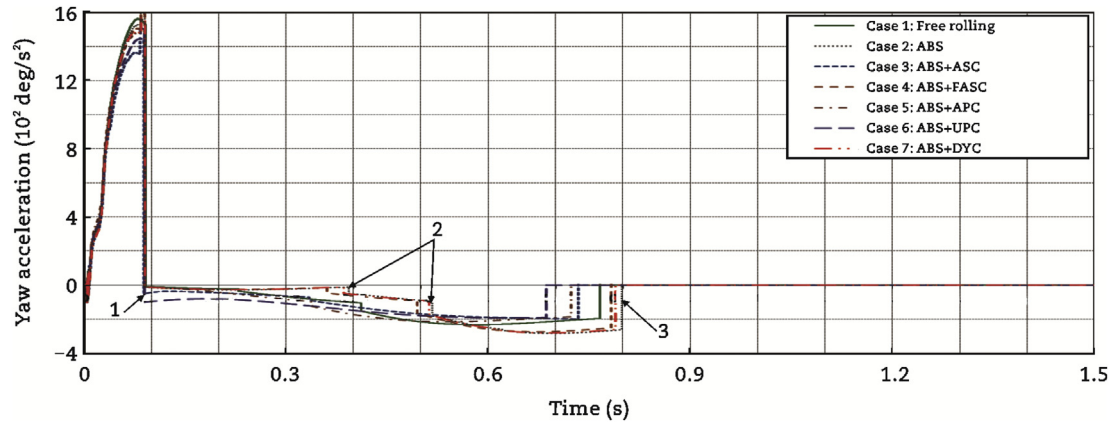


Fig. 16 – Vehicle body yaw acceleration (offset frontal vehicle-to-vehicle impact), vehicle (a).

observed in Case 1 (free rolling) as shown in Fig. 11, the greatest peak of yaw velocity appears in the same case as shown in Fig. 15. A reduction of the maximum yawing velocity (10 deg/s) is observed in Cases 3 and 6, while a reduction of about 5 deg/s is obtained in the other cases of VDCS.

Vehicle body yaw acceleration-time histories are depicted in Fig. 16. The maximum yaw acceleration is observed in Case 1 (free rolling) and the minimum yaw acceleration is also observed in Cases 3 and 6. At the end of the collision, the vehicle is controlled by the front-left wheel only, as mentioned before, trying to hinder the yawing motion. Accordingly, a negative yawing acceleration is generated with different small values related to each case as shown in Fig. 16 (arrow 1). These negative values of the vehicle yaw acceleration increase slowly with time producing two sudden drops of acceleration (arrow 2) once the right-rear wheel and the left-rear wheel re-contact the ground, respectively. These drops are not shown in Case 6 because the rear wheels do not leave the ground in this case. When the vehicle yawing ends and the yaw speed reaches zero, the yaw acceleration returns to zero as well as shown in Fig. 16 (arrow 3).

Fig. 17 shows the vehicle body yaw angle-time histories for all cases of vehicle (a). It is found that the maximum yaw angle of 49.3 deg is noticed in Case 2 (ABS) while the minimum yaw angle of 36.8 deg is noticed in Case 6 (ABS + UPC). The maximum value of the vehicle yaw angle depends on the maximum yaw acceleration and the vehicle pitch angle for each case. It is worth mentioning that reducing the maximum vehicle body yaw angle reduces the risk of the car side-impact by any obstacles on the road. Following the yawing analysis, it can be said that the best set of the vehicle dynamic control is to apply Case 6 (ABS + UPC) since the minimum yaw angle and acceleration are obtained in this case.

The yawing event of the vehicle (b), which is not equipped by the VDCS, is affected by vehicle (a) once different control systems are applied. The maximum yaw velocity of the vehicle (b) is increased in all cases compared with the free rolling case, except in Case 6. It is observed that the maximum yaw acceleration is also increased in all cases compared with the free rolling case by different values related to each case. In the same manner, the maximum yaw angle of the vehicle (b) is increased in all cases by different values (from 1.5 to 2 deg) related to each case, except in Case 6. However, all these values are very small and insignificant.

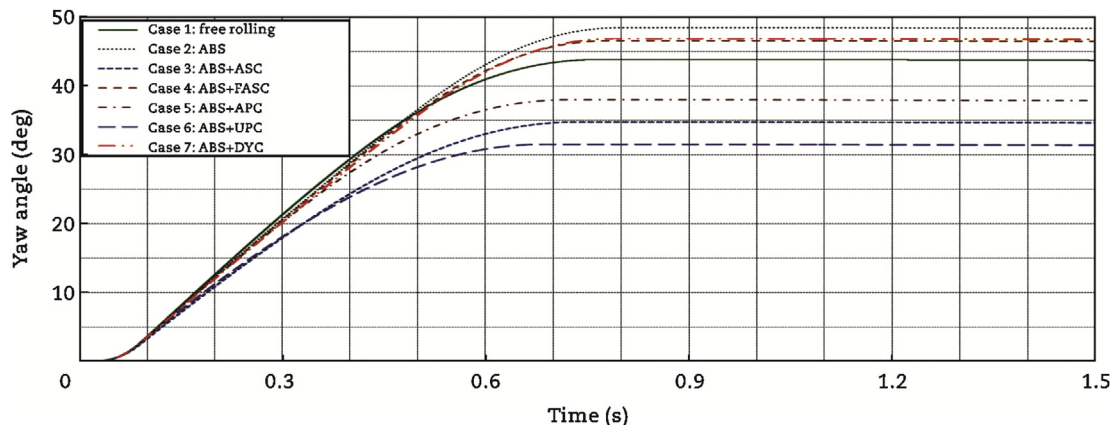


Fig. 17 – Vehicle body yaw angle (offset frontal vehicle-to-vehicle impact), vehicle (a).

**Table 2 – Values of the different parameters used in secondary impact simulations.**

Parameter	$m_1$ (kg)	$m_2$ (kg)	$m_3$ (kg)	$l_2$ (m)	$l_3$ (m)	$L_1$ (m)	$L_2$ (m)	$L_3$ (m)
Value	26.68	46.06	5.52	0.427	0.240	0.30	2.30	0.65
Parameter	$L_4$ (m)	$L_5$ (m)	$L_6$ (m)	$L_7$ (m)	$L_8$ (m)	$L_9$ (m)	$\beta$ (deg)	$\zeta$ (deg)
Value	0.30	0.35	0.45	0.55	0.97	1.10	30	15
Parameter	$\alpha$ (deg)	$\gamma$ (deg)	$\epsilon_1$ (deg)	$\epsilon_2$ (deg)	$\rho_1$ (deg)	$\rho_2$ (deg)	$k_{12}$ (N·m/rad)	
Value	23	30	15	15	35	43	380	
Parameter	$k_{23}$ (N·m/rad)	$k_1$ (N/m)	$k_2$ (N/m)	$k_3$ (N/m)	$k_4$ (N/m)	$k_5$ (N/m)	$k_6$ (N/m)	
Value	200	58,860	39,240	2500	2500	2500	2500	
Parameter	$c_1, c_2, c_3, c_4, c_5, c_6$		$d_{s1}, d_{s2}$ (m)		$d_{s3}, d_{s4}$ (m)		$d_{s5}$ (m)	$d_{s6}$ (m)
Value	20% of the critical damping		0.00		0.05		0.00	0.05

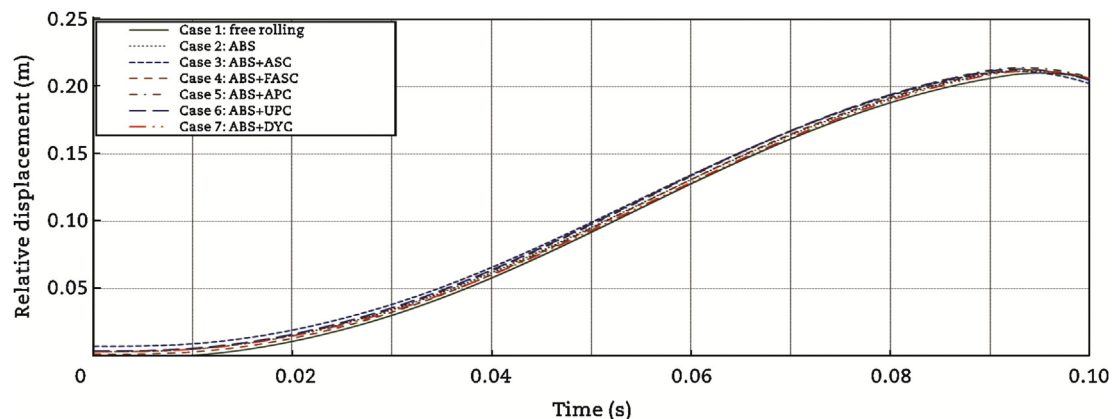
### 3.2. Secondary impact results

The secondary impact simulation results for offset vehicle-to-vehicle crash scenario are demonstrated in this section. The values of different parameters used in numerical simulations are given in Table 2, where  $d_{s1}$ ,  $d_{s2}$ ,  $d_{s3}$ ,  $d_{s4}$ ,  $d_{s5}$  and  $d_{s6}$  are the Initial slack lengths of the lower seatbelt, upper seatbelt, lower frontal airbag spring, upper frontal airbag spring, lower side airbag spring and upper side airbag spring, respectively. The values  $m_1$ ,  $m_2$ ,  $m_3$ ,  $l_2$ ,  $l_3$ ,  $k_{12}$  and  $k_{23}$  have been taken from (Ilie and Tabacu, 2010). Fig. 18 shows the occupant's pelvis relative displacement for vehicle (a). It is shown that it increases forward to reach its maximum position and then returns due to the lower seatbelt springs. It is observed that there are insignificant differences between the values of the maximum relative displacement of the occupant's pelvis. Related to the lower-body deceleration, it is shown that it increases during the collision to reach its maximum values at the end of impact and then reduces after the effect of collision is ended. It observed that the maximum deceleration is almost the same for all cases with very small differences. These small differences mean that the VDCS do have an insignificant effect on the pelvis relative displacement and deceleration.

The rotation angle of the occupant's chest about y axis for all cases of vehicle (a) is shown in Fig. 19. The occupant's chest

starts the collision with different rotational angles according to each case. The occupant takes this angle in the period of 1.5 s prior collisions when the VDCS is applied. After that, the rotational angle of the occupant's chest remains constant for about 0.03 s, then it increased to reach its maximum value after the end of the collision. The maximum rotation angle is observed in Cases 2, 4 and 7 while the minimum one is observed in Case 6 (ABS + UPC). Fig. 20 shows the rotational acceleration about y axis of the occupant's chest. The chest rotational acceleration increases gradually to reach its maximum positive value and then reduces to reach its maximum negative value. The maximum positive rotational acceleration is monitored in Case 1 and the minimum one occurred in Case 5, while the maximum negative rotational acceleration is shown in Case 6 and the minimum is in Cases 2 and 7.

The rotation angle of the occupant's head about y axis is depicted in Fig. 21. The head rotation angle increases rapidly for a period of time, which occurred during the increase of the chest rotation. And then, it increases fast due to the return of the occupant's chest to reach its peak value (maximum value). The peak value of the head rotational angle is observed in Cases 2, 4 and 7, while the minimum one is detected in Case 6. Fig. 22 shows the rotational acceleration of the occupant's head. The acceleration increases with a different manner according to each case to

**Fig. 18 – Occupant's pelvis displacement (offset frontal vehicle-to-vehicle impact), vehicle (a).**

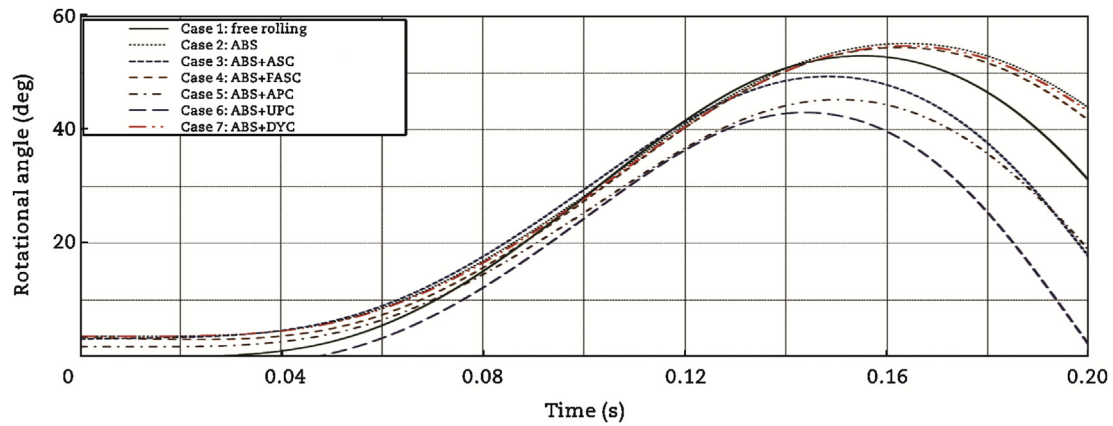


Fig. 19 – Rotational angle of the occupant's chest about y axis (offset frontal vehicle-to-vehicle impact), vehicle (a).

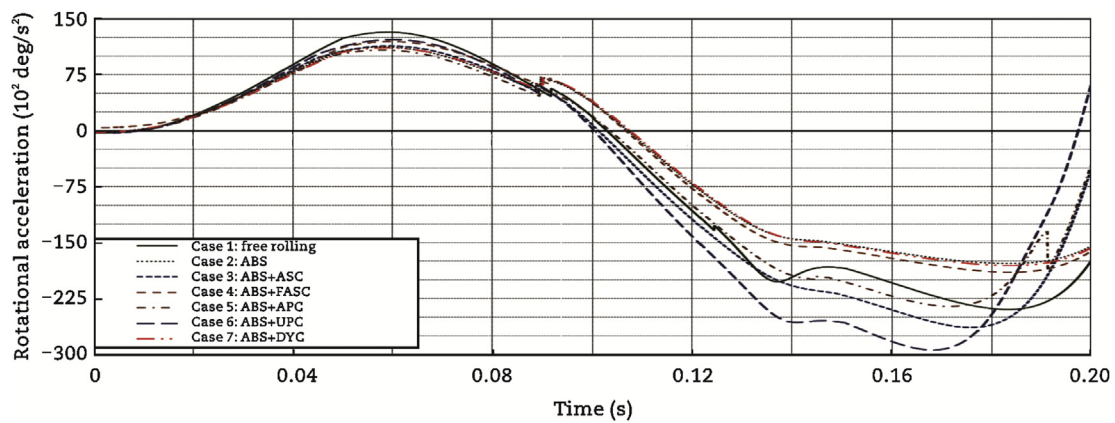


Fig. 20 – Rotational acceleration of the occupant's chest about y axis (offset frontal vehicle-to-vehicle impact), vehicle (a).

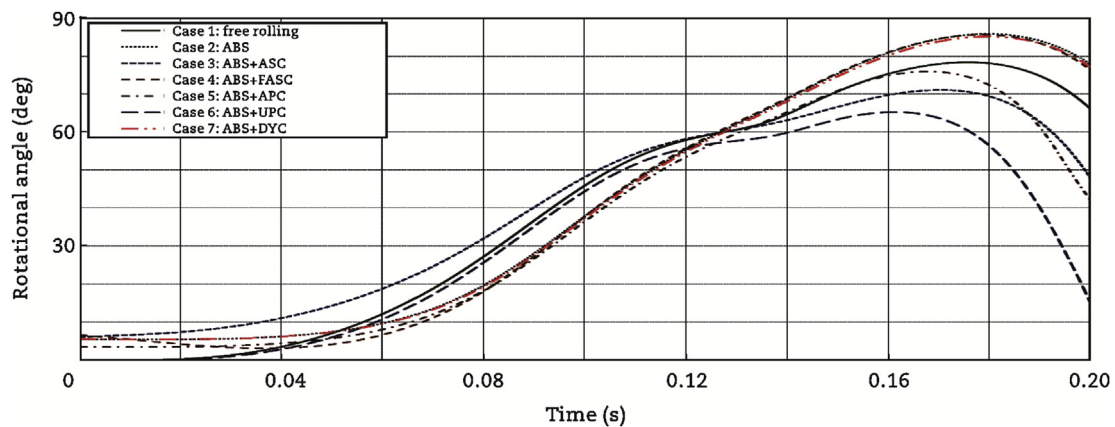


Fig. 21 – Rotational angle of the occupant's head about y axis (offset frontal vehicle-to-vehicle impact), vehicle (a).

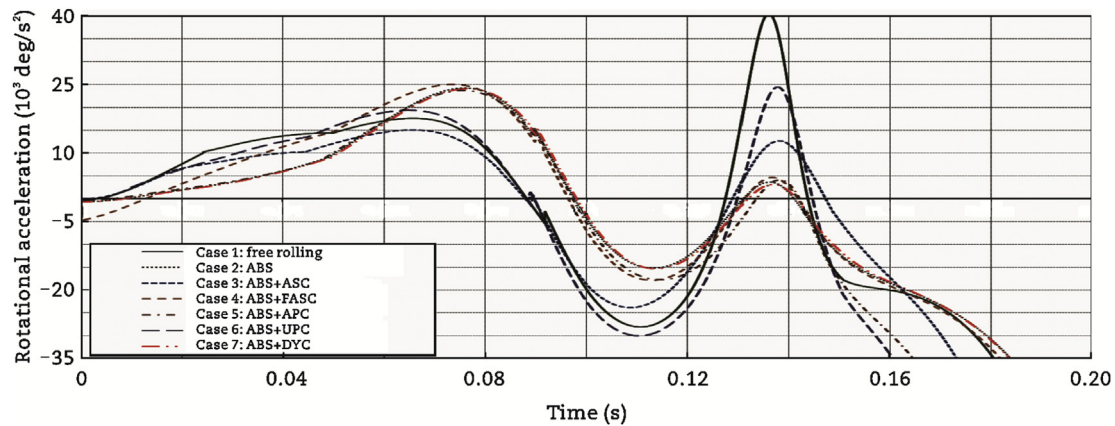


Fig. 22 – Rotational acceleration of the occupant's head about y axis (offset frontal vehicle-to-vehicle impact), vehicle (a).

reach its maximum value. These maximum values occurred in different time related to each case. In other words, the maximum acceleration in Cases 1, 3 and 6 occurs approximately at 0.07 s, while in the other cases it occurs approximately at 0.08 s. The minimum negative acceleration is observed in Cases 2 and 7, while the maximum negative values are seen in Cases 1 and 6.

The rotation angle about x axis of the occupant's chest for all cases of vehicle (a) is depicted in Fig. 23. When the occupant's chest reaches its maximum rotational angle, it stays in this position for a period of time while the vehicle rotates around the point of impact. The maximum rotation angle is observed in Case 1 (free rolling) while the minimum angle is observed in Cases 3 and 6 (ABS + ASC and ABS + UPC). Fig. 24 shows the rotational acceleration of the occupant's chest about x axis for all 6 cases for vehicle (a). The first sudden change in this acceleration is due to the activation of the side airbag, while the second one is due to the reverse braking force (arrows 1 and 2, respectively). The third sudden change of the chest acceleration (arrow 3) is due to the deactivation of the vehicle's front-end springs, which causes a sudden decrease of the vehicle pitching, yawing and rolling. The maximum positive rotational acceleration of the occupant's chest about x axis is observed

in Cases 1 and 7, while the minimum value occurs in Case 3. The maximum negative rotational acceleration happens in Cases 1 and 4 and the minimum is observed in Case 3. These negative acceleration values occur due to the force generated by the lower spring-damper system of the side airbag.

The rotation angle about x axis of the occupant's head for vehicle (a) is shown in Fig. 25. At the beginning of the collision, while the chest takes a positive acceleration and starts rotating towards the vehicle's side door, the head takes a different negative small rotation value related to each case, all these values are close to 5 deg. The positive maximum value of the head rotational angle is observed in Case 6, while the minimum peak angle is seen in Cases 2, 3, 4 and 7. Fig. 26 shows the rotational acceleration about x axis of the occupant's head for all cases. The effect of the reverse braking force is observed at the end of the collision (arrow 1 in Fig. 26). The maximum positive acceleration (in the period from 0.06 to 0.10 s) is almost the same for all cases, while the maximum negative acceleration (in the period from 0.10 to 0.16 s), caused by the side airbag force, is observed in Case 1 with relatively a higher value. The minimum negative acceleration is detected in Cases 2, 4, 5 and 7.

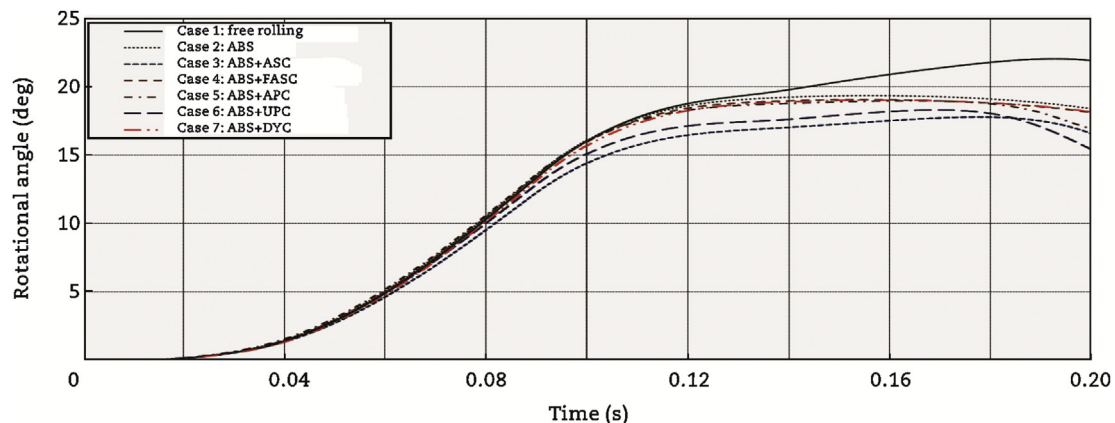


Fig. 23 – Rotational angle of the occupant's chest about x axis (offset frontal vehicle-to-vehicle impact), vehicle (a).



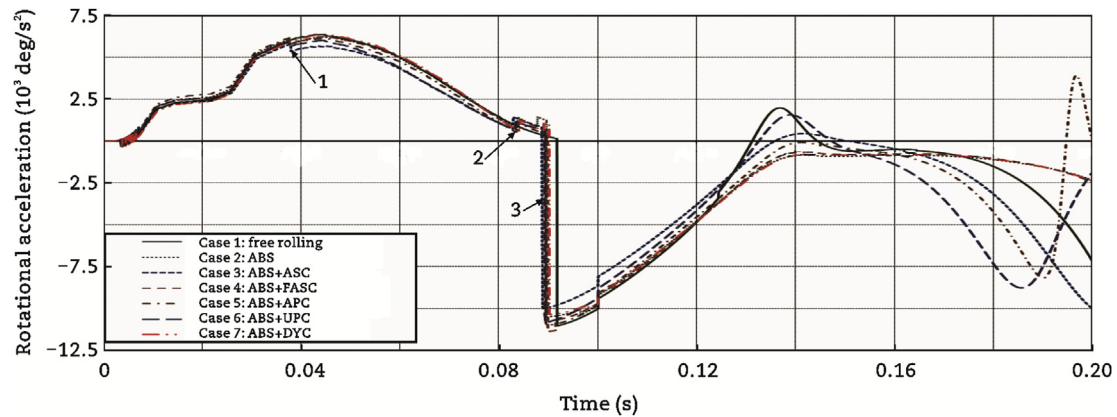


Fig. 24 – Rotational acceleration of the occupant's chest about x axis (offset frontal vehicle-to-vehicle impact), vehicle (a).

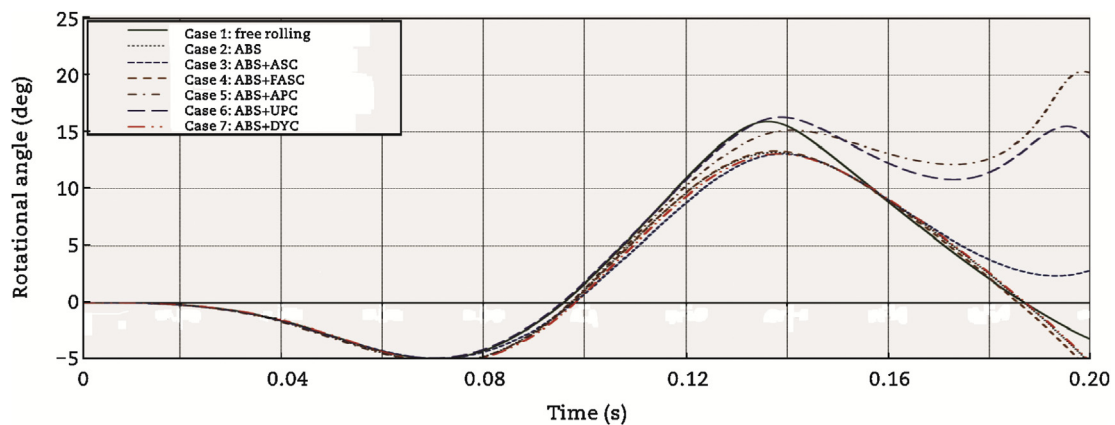


Fig. 25 – Rotational angle of the occupant's head about x axis (offset frontal vehicle-to-vehicle impact), vehicle (a).

It is shown that the occupant's pelvis relative displacement and deceleration for vehicle (b) are insignificantly affected by the application of VDCS on the other vehicle (vehicle (a)). There are very small and insignificant increases, especially on

the peak values, for all cases compared with the free rolling case.

The occupant's chest rotational angle for vehicle (b) and its acceleration about y axis are also obtained. It observed that

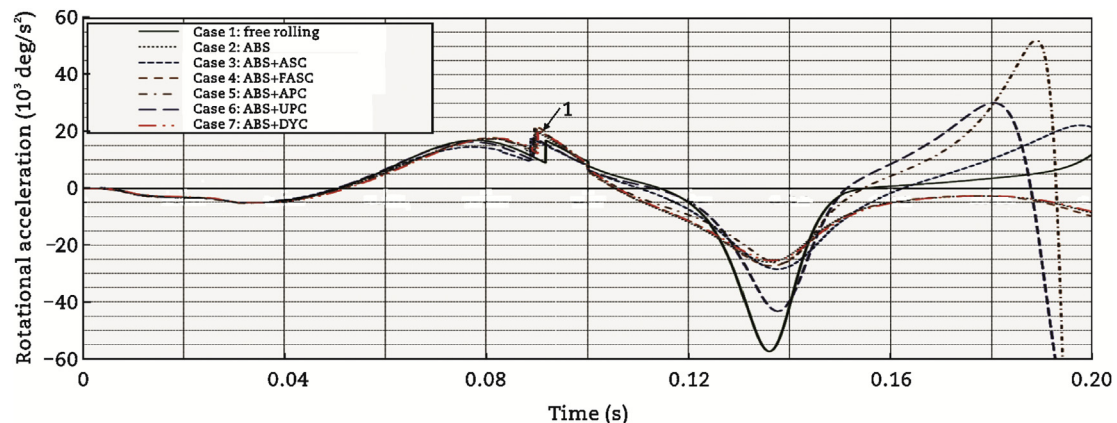
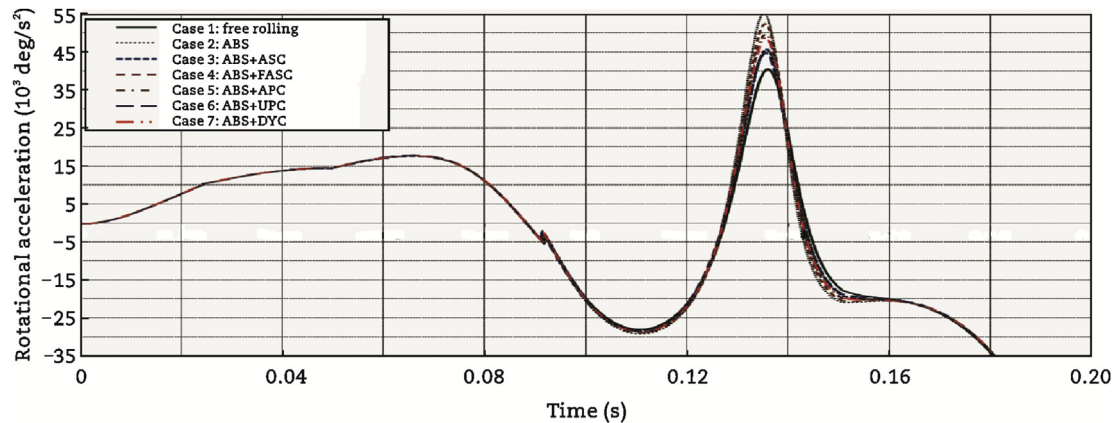


Fig. 26 – Rotational acceleration of the occupant's head about x axis (offset frontal vehicle-to-vehicle impact), vehicle (a).





**Fig. 27 – Rotational acceleration of the occupant's head about y axis (vehicle offset frontal vehicle-to-vehicle impact), vehicle (b).**

there are no changes in the rotational angle; however, there are small variations among the different cases on the occupant's chest acceleration from 0.13 to 0.15 s. These variations are also very small and insignificant.

The occupant's head rotational angle about y axis for the occupant in vehicle (b) is gained. It is shown that there are very small differences of the maximum rotational angle according to the different cases. Fig. 27 shows the occupant's head rotational acceleration about y axis for all cases. From this figure, a clear difference in the head rotational acceleration is detected at 0.135 s. When the VDCS is applied, the maximum head rotational acceleration becomes higher than the one in the free rolling case with different values from 5000 to 15,000  $\text{deg/s}^2$  related to each case; and the maximum head rotational acceleration is shown in Case 2.

The occupant's chest rotational angle about x axis for vehicle (b) is recorded. Compared with the free rolling case, the rotational angle of the chest is increased by small values from about 0.2 deg in Case 6 to about 2 degs in Cases 2 and 4. The occupant's chest acceleration about the x axis showed very small increases of the chest rotational acceleration when the VDCS were applied at the periods from 0.04 to 0.09 s and from 0.13 to 0.15 s. This increase in the chest rotational acceleration ranges between 300 and 800  $\text{deg/s}^2$ , however, these are not significant values.

The maximum occupant's head rotational angle about x axis is also increased when any of the VDCS is applied. This increase ranges between 0.2 and 1.0 deg, and this is not a significant value. The maximum head rotational angle is observed in Case 2, while the minimum value is detected in Case 1. The maximum positive acceleration of the occupant's head about x axis is almost the same. However, the maximum negative head rotational acceleration is increased when the VDCS are applied. In Case 6 the head rotational acceleration is increased by about 5000  $\text{deg/s}^2$ , while the highest increase value is observed in Case 2 by about 15,000  $\text{deg/s}^2$ .

#### 4. Conclusions

Development of a new 6-DOF vehicle dynamics/crash mathematical model and three dimensional-three-mass occupant

mathematical model has been represented to study the effect of vehicle dynamic control systems (VDCS) on vehicle crash at offset frontal vehicle-to-vehicle collision. The models presented here would be very useful in the early design stages for assessing the crash worthiness performance of the vehicle and for selecting appropriate vehicle parameters. From the numerical simulations, it can be said that the VDCS can improve the vehicle crash situation and the occupant behaviour. The different cases applied in this paper have a different effect on the vehicle and its occupant. It is shown that the crash event gets worse related to the vehicle (b), based on higher values of vehicle deceleration, pitching angle and acceleration, etc. However, these higher values are very small and insignificant.

#### Acknowledgments

The authors would like to thank the Egyptian government and the Faculty of Engineering, Ain Shams University for supporting this research. We also acknowledge with sadness, the contribution of Prof. Dave Crolla who has passed away during the period of this research.

#### REFERENCES

- Alleyne, A., 1997. Improved vehicle performance using combined suspension and braking forces. *Vehicle System Dynamics* 27 (4), 235–265.
- Alleyne, A., Hedrick, J.K., 1995. Nonlinear adaptive control of active suspensions. *IEEE Transactions on Control Systems Technology* 3 (1), 94–101.
- Bang, M.S., Lee, S.H., Han, C.S., et al., 2001. Performance enhancement of a sliding mode wheel slip controller by the yaw moment control. *Proceedings of the Institution of Mechanical Engineers Part D: Journal of Automobile Engineering* 215 (4), 455–468.
- Celentano, G., Iervolino, R., Porreca, S., et al., 2003. Car brake system modeling for longitudinal control design. In: *IEEE Conference on Control Applications, Hawaii, 2003*.

- Chang, J.M., Ali, M., Craig, R., et al., 2006. Important Modeling Practices in CAE Simulation for Vehicle Pitch and Drop. SAE International, Warrendale.
- Elkady, M., Elmarakbi, A., 2012. Modelling and analysis of vehicle crash system integrated with different VDCS under high speed impacts. *Central European Journal of Engineering* 2 (4), 585–602.
- Elmarakbi, A., Elkady, M., MacIntyre, J., 2013. Numerical analysis of vehicle-to-vehicle impact using vehicle dynamics control systems for collision mitigation. *International Journal of Dynamics and Control* 1 (2), 172–191.
- Elmarakbi, A., Zu, J., 2005. Crashworthiness improvement of vehicle-to-rigid fixed barrier in full frontal impact using novel vehicle's front-end structures. *International Journal of Automotive Technology* 6 (5), 491–499.
- Elmarakbi, A., Zu, J., 2007. Incremental harmonic balance method for analysis of standard/smart vehicles-to-rigid barrier frontal collision. *International Journal of Vehicle Safety* 2 (3), 288–315.
- Emori, R.I., 1968. Analytical Approach to Automobile Collisions. SAE International, Warrendale.
- Gietelink, O., Ploeg, J., De Schutter, B., et al., 2006. Development of advanced driver assistance systems with vehicle hardware-in-the-loop simulations. *International Journal of Vehicle Mechanics and Mobility* 44 (7), 569–590.
- Hogan, I., Manning, W., 2007. The use of vehicle dynamic control systems for automotive collision mitigation. In: *The 3rd Institution of Engineering and Technology Conference on Automotive Electronics*, Warwick, 2007.
- Ilie, S., Tabacu, Ș., 2010. Study of the Occupant's kinematics during the frontal impact. *Ann Oradea University, Fascicle Management Technology Engineering* 6 (16), 542–551.
- Jansson, J., Gustafsson, F., Ekmark, J., 2002. Decision Making for Collision Avoidance Systems. SAE International, Warrendale.
- Kamal, M.M., 1970. Analysis and Simulation of Vehicle to Barrier Impact. SAE International, Warrendale.
- Khatab, A., 2010. Steering System and Method for Independent Steering of Wheels (PhD thesis). Concordia University Montreal, Quebec.
- Kim, H.S., 2002. New extruded multi-cell aluminum profile for maximum crash energy absorption and weight efficiency. *Thin-Walled Structures* 40 (4), 311–327.
- Ori, T.R., Gbaha, P., Asseu, O., et al., 2011. Vehicle stopping distance by means of suspensions control. *Asian Journal of Scientific Research* 4 (1), 28–41.
- Pasillas-Lépine, W., 2006. Hybrid modeling and limit cycle analysis for a class of five-phase anti-lock brake algorithms. *Vehicle System Dynamics* 44 (2), 173–188.
- Seiler, P., Song, B., Hedrick, J., 1998. Development of a Collision Avoidance System. SAE International, Warrendale.
- Sugimoto, Y., Sauer, C., 2005. Effectiveness estimation method for advanced driver assistance system and its application to collision mitigation brake system. In: *The 19th International Technology Conference on the Enhanced Safety Vehicles*, Washington DC, 2005.
- Tamura, M., Inoue, H., Watanabe, T., et al., 2001. Research on a Brake Assist System with a Preview Function. SAE International, Warrendale.
- Witteman, W.J., 1999. Improved Vehicle Crashworthiness Design by Control of the Energy Absorption for Different Collision Situations (PhD thesis). Eindhoven University of Technology, Eindhoven.
- Witteman, W.J., Kriens, R.F.C., 1998. Modeling of an innovative frontal car structure: similar deceleration curves at full overlap, 40 percent offset and 30 degrees collisions. In: *16th*

*International Technical Conference on the Enhanced Safety of Vehicles*, Windsor, 1998.

Yu, F., Feng, J.Z., Li, J., 2002. A fuzzy logic controller design for vehicle abs with an on-line optimized target wheel slip ratio. *International Journal of Automotive Technology* 3 (4), 165–170.

Yue, C., Butsuen, T., Hedrick, J.K., 1988. Alternative control laws for automotive active suspensions. *Journal of Dynamic Systems, Measurement, and Control* 111 (2), 286–291.



**Mustafa Elkady** is an assistant professor of mechanical engineering at Lebanese International University (LIU). He received a competition grant from the Egyptian government (~£100,000 for 3 years) for his PhD. He obtained his PhD in mechanical engineering at the Department of Computing, Engineering and Technology, University of Sunderland, UK (2012). Prior to this he was a teaching assistant in mechanical engineering at the Automotive Department, Ain Shams University, Egypt. He obtained his Master degree in automotive engineering at Ain Shams University, Egypt (2004). His research interests include mathematical modelling analysis, advanced dynamics, vehicle dynamics, crash-worthiness, vehicle safety and impact biomechanics, vehicle engine controls and energy-efficient using lightweight materials. His research outcomes are realized as evident from his over 20 publications, he has published the book, *Enhancement of Vehicle Crash/Occupant Safety: Mathematical Modelling*.



**Ahmed Elmarakbi** obtained his PhD in mechanical engineering from the University of Toronto, Canada (2004). After successful postdoctoral fellowships in Canada and Japan, he moved to the University of Sunderland, UK in 2007, where he is, currently, a professor of automotive composites. His research interests lie in the area of energy-efficient and safe vehicles (EESVs) including advanced composite materials (e.g., graphene) for automotive applications and

low carbon vehicles. His work outcomes are recognized both nationally and internationally as evident from his 70+ plenary lectures, invited talks and presentations; 130+ peer-reviewed research papers. Most recently (2013), he has published the book: *Advanced Composite Materials for Automotive Applications: Structural Integrity and Crash-worthiness*, with Wiley, UK. He has 15 years of experience managing national and international projects, including multi-disciplinary collaborative projects with Europe, USA, Canada, China, Japan, and Brazil. He has received many prestigious awards and grants worldwide, including EU Graphene Flagship, Horizon2020, EPSRC, NSERC, JSPS, OGS, FP7, and several fellowships. He is expert reviewer for FP7 and EPSRC, member of several professional bodies; editorial-board member of high-impact international journals; organizer of international conferences and reviewer for conferences and many high-impact journals. He is also founder Editor-in-Chief of *International Journal of Automotive Composites*. He has an extensive track record of collaboration with the automotive industry and world-class

academic institutions over the last 15 years and he is currently a member of the EU Graphene Flagship.



**John MacIntyre** is the dean of the Faculty of Applied Sciences, and Pro Vice Chancellor at the University of Sunderland. He has worked at the University of Sunderland since 1992, having graduated from the University with a First Class Honours Degree in combined science (computer science and physiology). He then went on to complete a PhD in applied artificial intelligence, focussing on the use of neural networks in predictive maintenance, which was awarded in 1996. During 1990s

John established a research centre for adaptive systems at the university, which became recognized by the UK government as a centre of excellence for applied research in adaptive computing and artificial intelligence. The centre undertook many projects working with and for external organizations in industry, science and academia, and for three years ran the smart software for decision makers programme on behalf of the Department of Trade

and Industry. He has successfully supervised PhDs in fields ranging from neural networks, hybrid systems, and bioinformatics through to lean manufacturing, predictive maintenance, and business and maintenance strategies. He went on to become associate dean, and then the dean of the School of Computing, Engineering and Technology, covering computer science and engineering. In 2008 he became the dean of the Faculty of Applied Science, and in 2010 Pro Vice Chancellor of the University.



**Mohammad Alhariri** is a research assistant in the Department of Computing, Engineering and Technology and a PhD student in automotive engineering in the University of Sunderland. His research interests lie in the area of safety in passenger-vehicle. His current work focuses on developing a novel controller for vehicles dynamic systems aiming for better energy absorption resulting from vehicle frontal crashes.